Acta Crystallographica Section D
Biological Crystallography
ISSN 0907-4449

Structure and function of CYP108D1 from *Novosphingobium aromaticivorans* DSM12444: an aromatic hydrocarbon-binding P450 enzyme

Stephen G. Bell,[a]*‡§ Wen Yang,[b]‡ Jake A. Yorke,[a] Weihong Zhou,[b]* Hui Wang,[c] Jeffrey Harmer,[d] Rachel Copley,[a] Aili Zhang,[b] Ruimin Zhou,[b] Mark Bartlam,[b] Zihe Rao[b,c] and Luet-Lok Wong[a]

[a]Department of Chemistry, University of Oxford, Inorganic Chemistry Laboratory, South Parks Road, Oxford OX1 3QR, England, [b]College of Life Sciences and The State Key Laboratory of Medicinal Chemical Biology, Nankai University, Tianjin 300071, People's Republic of China, [c]Laboratory of Structural Biology, Tsinghua University, Beijing 100084, People's Republic of China, and [d]Centre for Advanced Electron Spin Resonance, Department of Chemistry, University of Oxford, Inorganic Chemistry Laboratory, South Parks Road, Oxford OX1 3QR, England

‡ These authors contributed equally to this work.
§ Current address: The School of Chemistry & Physics, University of Adelaide, North Terrace, Adelaide, SA 5005, Australia.

Correspondence e-mail: stephen.bell@chem.ox.ac.uk, stephen.bell@adelaide.edu.au, zhouwh@nankai.edu.cn

Received 12 September 2011
Accepted 12 January 2012

PDB Reference: CYP108D1, 3tkt.

CYP108D1 from *Novosphingobium aromaticivorans* DSM12444 binds a range of aromatic hydrocarbons such as phenanthrene, biphenyl and phenylcyclohexane. Its structure, which is reported here at 2.2 Å resolution, is closely related to that of CYP108A1 (P450terp), an α-terpineol-oxidizing enzyme. The compositions and structures of the active sites of these two enzymes are very similar; the most significant changes are the replacement of Glu77 and Thr103 in CYP108A1 by Thr79 and Val105 in CYP108D1. Other residue differences lead to a larger and more hydrophobic access channel in CYP108D1. These structural features are likely to account for the weaker α-terpineol binding by CYP108D1 and, when combined with the presence of three hydrophobic phenylalanine residues in the active site, promote the binding of aromatic hydrocarbons. The haem-proximal surface of CYP108D1 shows a different charge distribution and topology to those of CYP101D1, CYP101A1 and CYP108A1, including a pronounced kink in the proximal loop of CYP108D1, which may result in poor complementarity with the [2Fe–2S] ferredoxins Arx, putidaredoxin and terpredoxin that are the respective redox partners of these three P450 enzymes. The unexpectedly low reduction potential of phenylcyclohexane-bound CYP108D1 (−401 mV) may also contribute to the low activity observed with these ferredoxins. CYP108D1 appears to function as an aromatic hydrocarbon hydroxylase that requires a different electron-transfer cofactor protein.

1. Introduction

The cytochromes P450 (CYPs) are a superfamily of haem-containing monooxygenases that are found in virtually all living organisms (Ortiz de Montellano, 2005; Sigel *et al.*, 2007). P450 enzymes accept a diverse range of substrates, resulting in many functional roles, including the biosynthesis of endogenous compounds, the degradation of xenobiotics and drug metabolism. Their primary function is C—H bond oxidation, although other reactions such as dealkylation, phenol coupling, alkene epoxidation, heteroatom oxidation and reductive dehalogenation have also been reported (Guengerich, 2001; Cryle *et al.*, 2003; Isin & Guengerich, 2007). P450 enzymes are drug targets and their potential applications in the synthesis of drug metabolites and fine chemicals have led to sustained efforts to discover new activity and to understand their substrate specificity and protein-recognition interactions

with electron-transport proteins for the reconstitution of high substrate oxidation activity.

Novosphingobium aromaticivorans DSM12444 is a Gram-negative strictly aerobic bacterium found in soil, water and coastal plain sediments (Takeuchi *et al.*, 2001). It is able to metabolize and degrade polyaromatic hydrocarbons and other aromatic contaminants (Fredrickson *et al.*, 1991) and has been reported to be a potential initiator of primary biliary cirrhosis (Kaplan, 2004). Its genome revealed many genes involved in the catabolism of aromatic compounds distributed over the chromosomal DNA and two large plasmids pNL1 (180 kbp) and pNL2 (480 kbp) (http://genome.jgi-psf.org/finished_microbes/novar/novar.home.html; Romine *et al.*, 1999). Therefore, *N. aromaticivorans* and its enzymes have potential uses in biocatalysis and bioremediation. We have investigated the monooxygenase enzymes from this bacterium in order to assess their potential for applications in C—H bond oxidation. 16 potential cytochrome P450 genes that belong to 12 different cytochrome P450 families have been identified. The production, purification and screening of potential substrates for the majority of these CYP enzymes have been reported (Bell & Wong, 2007). The substrate range of the *N. aromaticivorans* cytochrome P450 complement is broad and includes monoterpenoids, sesquiterpenoids, alkanes, polyaromatic hydrocarbons and chlorinated benzenes (Bell & Wong, 2007).

A class I electron-transfer system from *N. aromaticivorans* consisting of an NADH-dependent ferredoxin reductase (ArR) and a [2Fe–2S] ferredoxin (Arx) has been shown to support the monooxygenase activity of CYP111A2 and the four CYP101 enzymes from this bacterium (Bell, Dale *et al.*, 2010; Yang *et al.*, 2010). The crystal structures of CYP101C1, CYP101D1, CYP101D2, ArR and Arx have been reported (Ma *et al.*, 2011; Yang *et al.*, 2010, 2011). These structures, and the kinetic behaviour of the enzymes, reveal that electrostatic interactions are likely to be important in protein–protein recognition, binding and electron transfer (Yang *et al.*, 2010).

CYP108D1 from *N. aromaticivorans* (UniProt Q2G3H6) is a homologue of P450terp (CYP108A1) from a *Pseudomonas* species (Fruetel *et al.*, 1994). The crystal structure of CYP108A1, which hydroxylates α-terpineol to yield 7-hydroxyterpineol, has been reported and its substrate-binding mode has been modelled (Hasemann *et al.*, 1994). α-Terpineol also binds to CYP108D1, but the haem spin state only shifts to 40% high spin compared with >95% high spin in CYP108A1. Unusually, CYP108D1 shows large haem spin-state shifts with aromatic hydrocarbons such as phenanthrene (90%), fluorene (70%), *p*-cymene (60%) and naphthalene (50%) (Bell & Wong, 2007). The activity of CYP108D1 is low when coupled to Arx and other [2Fe–2S] ferredoxins such as putidaredoxin (Pdx) from the CYP101A1 system (Bell & Wong, 2007) and terpredoxin (Tdx), the electron-transfer partner of CYP108A1 (Peterson *et al.*, 1992). In order to better understand the preference of CYP108D1 for more hydrophobic substrates and its low activity with the [2Fe–2S] ferredoxins tested, we have solved its crystal structure at 2.2 Å resolution and studied its substrate binding, redox properties and enzyme kinetics in more detail.

2. Methods

2.1. General

General DNA and microbiological experiments were carried out by standard methods (Sambrook *et al.*, 1989). The genomic DNA of *N. aromaticivorans* (ATCC 700278D-5) was obtained from ATCC-LGC Promochem, UK. KOD polymerase, which was used for the PCR steps, and the pET28a vector were from Merck Biosciences, UK; other enzymes for molecular biology were from New England Biolabs, UK. General reagents and organic substrates and product standards were from Sigma–Aldrich or Merck, UK. NADH and yeast alcohol dehydrogenase were from Roche Diagnostics, UK. Isopropyl β-D-1-thiogalactopyranoside (IPTG), growth media and buffer components were from Melford Laboratories, UK, Invitrogen, USA or the Beijing Chemical Company, People's Republic of China.

2.2. Cloning, expression and purification

The gene encoding full-length CYP108D1 was cloned into the vector pET28a(+) using the *Nde*I and *Hin*dIII restriction sites in order to incorporate an N-terminal 6×His tag (Bell & Wong, 2007). The protein was then produced using *Escherichia coli* strain BL21 (DE3). The cells were grown in LB medium containing 30 mg l^{-1} kanamycin at 310 K for 5 h and recombinant protein production was induced with 0.5 m*M* IPTG for 10 h at 301 K. The cells were harvested by centrifugation, resuspended in phosphate-buffered saline buffer pH 7.4 (PBS) and lysed by sonication at 277 K. The crude extracts were centrifuged at 20 000*g* for 1 h to remove cell debris and the soluble fraction was loaded onto an Ni^{2+}-chelating affinity column (2 ml; GE Healthcare, USA) pre-equilibrated with PBS. The column was washed with PBS containing 20 m*M* imidazole and the protein was eluted from the column using PBS containing 300 m*M* imidazole. CYP108D1 was buffer-exchanged into buffer *A* (20 m*M* Tris pH 8.0) before being loaded onto a Resource Q column (1 ml; GE Healthcare). The protein was eluted using a linear gradient of 0–1 *M* NaCl in buffer *A*. A Superdex 200 size-exclusion chromatography column (10 × 300 mm; GE Healthcare) was used for further purification and was eluted with buffer *A* containing 150 m*M* NaCl. The purity of CYP108D1 was estimated to be greater than 95% by SDS–PAGE analysis (Supplementary Fig. S1*a*[1]), which corresponds to an A_{418}/A_{280} ratio of ∼1.9 (Supplementary Fig. S1*b*[1]). The concentration of CYP108D1 was estimated using $\varepsilon_{446-490}$ = 91 mM^{-1} cm^{-1} for the CO difference spectrum (Omura & Sato, 1964). Using this value, the extinction coefficient for the ferric resting state of CYP108D1 was estimated to be ε_{417} = 111 mM^{-1} cm^{-1}.

Site-directed mutagenesis of CYP108D1 was performed using the Stratagene QuikChange mutagenesis kit with the primer 5′-CGACCCGACGCGC**GTG**GCCAACCGCCATC-TG-3′ and its reverse complement to generate the Pro365Val

[1] Supplementary material has been deposited in the IUCr electronic archive (Reference: KW5040). Services for accessing this material are described at the back of the journal.

Table 1
Data-collection and refinement statistics.

Values in parentheses are for the highest resolution shell.

Data-collection statistics	
Space group	*R*32
Unit-cell parameters (Å)	$a = b = 93.9$, $c = 299.3$
Wavelength (Å)	1.5418
Resolution (Å)	50–2.2 (2.28–2.20)
$\langle I/\sigma(I)\rangle$	24.3 (4.5)
Completeness (%)	100 (100)
Average multiplicity	7.3 (7.2)
$R_{\rm merge}$† (%)	8.3 (40.1)
Structure-refinement statistics	
Resolution (Å)	50–2.2
Average *B* factor (Å^2)	27.7
$R_{\rm work}/R_{\rm free}$‡ (%)	18.7/23.4
R.m.s. deviation from ideal bond lengths§ (Å)	0.017
R.m.s. deviation from ideal bond angles§ (°)	1.758
Ramachandran favoured (%)	96.31
Ramachandran outliers (%)	0.00
MolProbity score	2.41
Poor rotamers (%)	7.60
Clash scores	9.35

† $R_{\rm merge} = \sum_{hkl}\sum_i |I_i(hkl) - \langle I(hkl)\rangle|/\sum_{hkl}\sum_i I_i(hkl)$, where $I_i(hkl)$ is the *i*th intensity measurement of reflection *hkl* and $\langle I(hkl)\rangle$ is the average intensity from multiple observations. ‡ $R_{\rm work}/R_{\rm free} = \sum_{hkl}\big||F_{\rm obs}| - |F_{\rm calc}|\big|/\sum_{hkl}|F_{\rm obs}|$, where $F_{\rm obs}$ and $F_{\rm calc}$ are the observed and calculated structure factors, respectively. § Ideal values are derived from Engh & Huber (1991).

mutant (the mutated triplet codon is highlighted in bold; Eurofins MWG Operon, UK). The mutation was confirmed by DNA sequencing (Geneservice, Oxford University). The gene encoding full-length terpredoxin (Tdx) was provided in the vector pET23a(+) by Professor Tom Pochapsky (Mo *et al.*, 1999). The protein was produced and purified according to the published protocol for PuxB from *Rhodopseudomonas palustris* (except that the antibiotic in the growth medium was changed to ampicillin; Bell, Xu *et al.*, 2010) and the purity of Tdx was assessed by UV–Vis spectroscopy (Mo *et al.*, 1999). Other proteins used in this study were produced and purified as described previously (Bell, Dale *et al.*, 2010; Bell *et al.*, 2001; Bell, Xu *et al.*, 2010; Peterson *et al.*, 1990; Xu *et al.*, 2009). Proteins were stored at 253 K in 50 m*M* Tris pH 7.4 containing 50%(*v*/*v*) glycerol.

2.3. Crystallization and data collection

The purified CYP108D1 protein was concentrated to 40 mg ml^{-1} in crystallization buffer (20 m*M* Tris pH 8.0). Crystals of CYP108D1 were obtained using the hanging-drop vapour-diffusion method at 291 K. 1 µl protein solution (40 mg ml^{-1}) was mixed with 1 µl reservoir solution (0.2 *M* lithium sulfate, 0.1 *M* Tris pH 8.3, 27% PEG 4000) and equilibrated against 300 µl of the same solution. Diffraction-quality crystals were obtained after approximately one week. X-ray diffraction data were collected on a Rigaku R-AXIS IV^{++} image plate using Cu *Kα* radiation (λ = 1.5418 Å) from an in-house Rigaku MicroMax-007 rotating-anode X-ray generator operating at 40 kV and 20 mA. The crystals were cryoprotected by addition of 20%(*v*/*v*) glycerol to the reservoir solution. The diffraction data set was indexed, integrated and scaled with the *HKL*-2000 package (Otwinowski & Minor, 1997). The crystals belonged to space group *R*32, with unit-cell parameters $a = 93.9$, $b = 93.9$, $c = 299.3$ Å. Complete data-collection statistics are summarized in Table 1.

2.4. Structure determination and refinement

For the structure determination of CYP108D1, the phases were solved by the molecular-replacement (MR) method using the program *Phaser* in the *CCP*4 suite (McCoy *et al.*, 2007; Winn *et al.*, 2011). The structure of CYP108A1 (PDB entry 1cpt; Hasemann *et al.*, 1994) was used as a search model. The initial model was rebuilt with *Coot* (Emsley & Cowtan, 2004) and refined with *ARP*/*wARP* (Perrakis *et al.*, 1999) and *REFMAC*5 (Murshudov *et al.*, 2011). The stereochemical quality of the refined structure was checked with the program *MolProbity* (Chen *et al.*, 2010). A summary of the structure-refinement statistics is provided in Table 1. The coordinates of the crystal structure of CYP108D1 have been deposited in the PDB (http://www.pdb.org; Berman *et al.*, 2000) with accession code 3tkt.

2.5. Substrate-docking experiments

Phenylcyclohexane and phenanthrene were docked into the structure of CYP108D1 using *AutoDock* 4 (Morris *et al.*, 1998). Preparation of the macromolecule and ligands was performed using the *AutoDock Tools* program. The grid box was centred on the active site of CYP108D1 and the docking search was carried out using the genetic algorithm method. *AutoGrid* and *AutoDock* were run using the default parameters of the program. A total of 50 simulations were run and the lowest-energy docking solutions were chosen for further analysis.

2.6. Substrate binding

Glycerol was removed immediately before use by gel filtration on a 5 ml PD-10 column (GE Healthcare) eluted with 50 m*M* Tris pH 7.4. UV–Vis spectra and spectroscopic activity assays were recorded at 303 ± 0.5 K on a Varian CARY-50 or CARY-1E spectrophotometer. For substrate-binding assays the CYP108D1 enzyme was diluted to ∼0.5 µ*M* in 50 m*M* Tris pH 7.4 (2.5 ml). Aliquots of substrate (0.5–2 µl) were added using a Hamilton syringe from a 1, 10 or 100 m*M* stock solution in DMSO. The sample was mixed and the spectrum was acquired between 700 and 250 nm and the peak-to-trough difference in absorbance was recorded. Further aliquots of substrate were added until the peak-to-trough difference did not shift further. The dissociation constants $K_{\rm d}$ were obtained by fitting the peak-to-trough difference, scaled for dilution, against substrate concentration to a hyperbolic function,

$$\Delta A = \frac{\Delta A_{\rm max} \times [S]}{K_{\rm d} + [S]}, \qquad (1)$$

where ΔA is the peak-to-trough absorbance difference, $\Delta A_{\rm max}$ is the maximum absorbance difference and $[S]$ is the substrate concentration.

Table 2
GC oven parameters.

Substrate	CP-Sil	DVF-wax
p-Cymene	333 K for 1 min, raise to 423 K at 15 K min^{-1}, hold for 3 min and then raise to 493 K over 1 min and hold for a further 2 min	373 K for 2 min, raise to 473 K at 5 K min^{-1} and hold for 13 min
α-Terpineol	As *p*-cymene	As *p*-cymene
Phenylcyclohexane	As *p*-cymene	As *p*-cymene
Naphthalene	As *p*-cymene	373 K for 2 min, raise to 523 K at 5 K min^{-1} and hold for 3 min
Fluorene	As *p*-cymene	373 K for 2 min, raise to 523 K at 5 K min^{-1} and hold for 13 min
Biphenyl	As *p*-cymene	As fluorene
Phenanthrene	373 K for 1 min, raise to 523 K at 10 K min^{-1} and hold for 13 min	As fluorene

Several substrates exhibited tight binding, with $K_d < 5[E]$, and in these instances the data were fitted to the tight-binding quadratic equation (Williams & Morrison, 1979),

$$\frac{\Delta A}{\Delta A_{max}} = \frac{([E] + [S] + K_d) - \{([E] + [S] + K_d)^2 - 4[E][S]\}^{1/2}}{2[E]}, \quad (2)$$

where ΔA is the peak-to-trough absorbance difference, ΔA_{max} is the maximum absorbance difference, $[S]$ is the substrate concentration and $[E]$ is the enzyme concentration.

The high-spin haem content was estimated (to approximately ±5%) by comparison with a set of spectra generated from the sum of the appropriate percentages of the spectra of the substrate-free form (>95% low spin, Soret maximum at 418 nm) and the camphor-bound form (>95% high spin, Soret maximum at 392 nm) of wild-type CYP101A1.

2.7. Product formation

NADH turnover-rate assays were performed with mixtures (1.2 ml) consisting of 50 m*M* Tris pH 7.4, 0.5 µ*M* CYP108D1, 5 µ*M* ferredoxin, 0.5 µ*M* ferredoxin reductase and 100 µg ml^{-1} bovine liver catalase. The mixtures were equilibrated at 303 K for 2 min. Substrates were added as a 100 m*M* stock solution in ethanol or DMSO to a final concentration of 0.2–1 m*M* depending on the substrate solubility. NADH was added to ~320 µ*M* (final A_{340} = 2.00) and the absorbance at 340 nm was monitored. The rate of NADH consumption was calculated using ε_{340} = 6.22 mM^{-1} cm^{-1}.

Substrate turnovers for product identification were carried out using the ArR–Arx electron-transfer system *in vitro*. The reactions were performed in 50 m*M* Tris pH 7.4 (final volume of 10 ml) using 100 n*M* of the appropriate CYP enzyme, 500 n*M* Arx, 100 n*M* ArR, 100 µg ml^{-1} bovine liver catalase, 100 µ*M* NADH and 90 units of yeast alcohol dehydrogenase (0.3 mg) as the cofactor-regenerating system. Substrate from a 1:1 ethanol:DMSO stock (final concentration 0.1–1 m*M*) was added. After stirring for 4 h at ambient temperature, the reaction was terminated by freezing. Products were extracted using ethyl acetate (EtOAc) and identified by co-elution of the extracts with authentic standards. 4-Phenylcyclohexanol isomers were produced by reducing 4-phenylcyclohexanone with excess $NaBH_4$ in EtOH. The reaction was quenched with H_2O before removing volatiles by evaporation. The organics were extracted using EtOAc. The different 4-phenylcyclohexanol isomers were identified by co-elution of the samples with a turnover of the CYP101A1 Y96F/V247L mutant with phenylcyclohexane (conditions as above) using PdR and Pdx as the electron-transfer proteins, which produced a tenfold excess of *trans*-4-phenylcyclohexanol over the *cis* isomer (Jones *et al.*, 1996; Bell *et al.*, 1997). 7-Hydroxyterpineol was produced by adding β-pinene oxide (2 mg) to a slight excess of $Hg(NO_3)_2$ in a 1:1 mixture of 50 m*M* Tris pH 7.4 and THF (4 ml) (Bluthe *et al.*, 1980; Fruetel *et al.*, 1994). The mixture was extracted using EtOAc.

Gas-chromatography (GC) analyses were performed on a ThermoFinnegan Trace GC instrument equipped with an auto-sampler and a CP-Sil 8 fused-silica column (15 m × 0.25 mm; Varian) or a ThermoFinnegan GC8000^{top} equipped with a DVF-wax fused-silica column (15 m × 0.25 mm; Varian) both using helium as the carrier gas and flame ionization detection. The injector and flame ionization detector were held at 473 and 523 K, respectively (523 and 553 K for larger polyaromatic hydrocarbons). The oven parameters are given in Table 2. The retention times for the substrates and products on the DVF-wax column were (retention times on the CP-Sil 8 column are given in parentheses): 18.8 (8.35) min for fluorene, 25.1 (9.2) min for 9-fluorenone, 29.1 (9.3) min for 9-hydroxyfluorene, 12.9 (6.85) min for biphenyl, 23.8 (7.9) min for 2-hydroxybiphenyl, 31.9 (9.0) min for 3-hydroxybiphenyl, 32.3 (9.1) min for 4-hydroxybiphenyl, 7.9 (4.9) min for α-terpineol, 22.6 (7.5) min for 7-hydroxyterpineol, (4.3) min for β-pinene oxide, 4.1 (3.0) min for *p*-cymene, 15.5 (6.05) min for 4-isopropylbenzylalcohol, 17.2 (6.0) min for thymol, 17.6 (6.15) min for carvacrol, 10.9 (4.9) min for *p*-α,α-trimethylbenzylalcohol, 7.4 (6.2) min for phenylcyclohexane, 19.2 (8.1) min for 4-phenylcyclohexanone, 21.2 (8.2) min for *trans*-4-phenylcyclohexanol, 20.6 (8.2) min for *cis*-4-phenylcyclohexanol, 8.6 (4.8) min for naphthalene, 28.2 (7.8) min for 1-naphthol, 29.1 (7.9) min for 2-naphthol, 24.7 (9.45) min for phenanthrene, 31.3 min for 2-phenanthrol, 30.4 min for 9,10-phenanthrenequinone and 29.4 min for 9-phenanthrol.

2.8. Redox titrations

Redox titrations were carried out in a custom-built optically transparent thin-layer electrode (OTTLE) cell constructed from a quartz cuvette of 0.1 cm path length as described previously (Whitehouse *et al.*, 2010, 2011). Anaerobic condi-

tions were maintained by purging the system continually with argon that had been sparged through an ~10 cm column of water at room temperature. The cell was held at 298 ± 0.1 K. The sample volume was approximately 1300 µl, comprising ~50–100 µ*M* protein, 5 µ*M* each of methylene blue, anthraquinone-1,5-disulfonate, anthraquinone-2,6-disulfonate, anthraquinone-2-sulfonate and methyl viologen, 10 m*M* glucose, 0.2 mg ml^{-1} glucose oxidase, 0.2 mg ml^{-1} catalase, 200 m*M* NaCl in 50 m*M* Tris pH 7.4 and, for titrations with the substrate-bound forms, 1 m*M* camphor, 500 µ*M* phenylcyclohexane and 2%(*v*/*v*) DMSO. Glucose, glucose oxidase and catalase were included to convert residual dioxygen to water. Sample preparation and cell assembly took place in a Belle Technology glove box (O_2 < 5 p.p.m.). Spectra were acquired for at least 40 min to allow equilibration. Longer periods produced no further changes to the spectrum within the sensitivity of the spectrometer. Data were corrected for baseline drifts by a zeroth-order adjustment based on the average optical density from 775 to 800 nm. Because the absorbance of the peaks in the Soret band was convoluted by contributions from the reduced form of methyl viologen (λ_{max} = 395 nm), the absorbances at 450, 465 and 550 nm were used for data analysis of the P450 enzymes and those at 415 and 460 nm for the Arx ferredoxin. Data were fitted to a sigmoid derived from the Nernst equation

$$A(E) = \frac{A(E_{max}) - A(E_{min})}{1 + \exp[(E_m - E_{appl})/(RT/nF)]} + A(E_{min}), \qquad (3)$$

where $A(E)$ is the absorbance for a given potential, $A(E_{max})$ and $A(E_{min})$ are the optical densities for the fully oxidized and fully reduced chromophore, E_m and E_{appl} are the midpoint and applied potentials, R is the gas constant, T is the cell temperature, n is the number of electrons transferred for the redox couple and F is Faraday's constant. The values of $A(E_{max})$, $A(E_{min})$ and E_m were determined by minimizing the square of the difference between the measured value and the predicted value, assuming equal weighting of the data. The value of n was fixed at 1. When n was allowed to vary, values ranged from 0.86 to 1.24. All potentials relate to the standard hydrogen electrode.

2.9. Stopped-flow spectrophotometry

The rate constants for the formation of the $Fe^{II}(CO)$ complex, k_f, for CYP101D1 and CYP108D1 in the presence of camphor and phenylcyclohexane were measured at 303 ± 0.1 K by monitoring the absorbance at 450 nm using an Applied Photophysics SX20 stopped-flow spectrophotometer operating in single-wavelength mode in a glove box. Components were prepared in 50 m*M* Tris pH 7.4 saturated with CO by gently bubbling for 5 min and then purging the headspace for a further 5 min. Syringe *A* contained 0.2 µ*M* ArR, 2–40 µ*M* pre-reduced Arx (by the addition of NADH) and syringe *B* the appropriate CYP enzyme (2 µ*M*) and the substrate (1 m*M* camphor or 500 µ*M* phenylcyclohexane) in 2%(*v*/*v*) ethanol. The components were mixed in a 1:1 ratio.

Data for CYP101D1 with camphor were fitted using the *Pro-Data Viewer* software (Applied Photophysics). At a final concentration of 2.5 µ*M* Arx and 1 µ*M* CYP101D1, the early part of the data could be fitted to a single exponential with a rate constant of 22.9 ± 0.8 s^{-1}. Although the relative amplitude of this phase varied between experiments, the rate constant derived from multiphasic fits always fell within a narrow range for each enzyme.

2.10. EPR

CW EPR experiments were performed using an X-band Bruker BioSpin GmbH EMX spectrometer equipped with a high-sensitivity Bruker probehead and an Oxford Instruments CF935 helium-flow cryostat. Experiments were conducted at 20 K with 0.2–2 mW microwave power, 0.5 mT modulation amplitude, a microwave frequency of 9.3909 GHz and a modulation frequency of 100 kHz.

3. Results and discussion

3.1. Overall structure of CYP108D1

The crystal structure of CYP108D1 was solved at 2.2 Å resolution using the molecular-replacement method, with the crystallographic R_{work} and R_{free} converging to 18.7% and 23.4%, respectively (Table 1). The final model is composed of one CYP108D1 molecule and 267 water molecules and adopts the characteristic P450 fold with a mixed α/β structure (Fig. 1*a*; Poulos *et al.*, 1987). CYP108D1 was traced from residues 4 to 430, with the exception of residues 192–209 of the *F*–*G* loop, and consists of 18 α-helices, four 3_{10}-helices and nine β-sheets. It shares both high sequence similarity (41% identity and 60% similarity) and structure similarity (r.m.s.d. = 1.2 Å for all C^{α} atoms) to CYP108A1 (Supplementary Figs. S2–S4; Hasemann *et al.*, 1994). The *F*–*G* loop was also not resolved in the CYP108A1 structure, but a high degree of flexibility in this region is common among P450 structures (Hasemann *et al.*, 1995; Pochapsky *et al.*, 2010). CYP108D1 contains fewer β-sheets than CYP108A1, and those that are present are shorter (Supplementary Fig. S2).

3.2. The access channel and the active site

An access channel is observed in the CYP108D1 crystal structure (Fig. 1*b*), the entrance of which is comprised of residues from the *B*′ and *F* helices as well as the *B*–*B*′ and *B*′–*C* loops. The entrance cannot be defined precisely because the unresolved *F*–*G* loop may act as a flexible 'lid' and cover the observed access channel (Hasemann *et al.*, 1994; Dunn *et al.*, 2001; Yang *et al.*, 2011). The *B*′ helix and the *B*–*C* and *F*–*G* loops are proposed to be important in substrate recognition and entry and therefore substrate specificity (Cojocaru *et al.*, 2007; Li & Poulos, 2004; Bell *et al.*, 2008). The positions of the *B*′, *F* and *G* helices and the C-terminus of the *I* helix are broadly similar to those in CYP108A1. There is a small change in the position of the *F* helix in CYP108D1 compared with CYP108A1, with the N-terminus in CYP108D1 being closer to the haem and the active site (Fig. 1*c*). The access channel is

hydrophobic and is flanked by the residues Val80, Thr82, Gly86, Ala90, Leu100 and Phe190 (Fig. 1*d*). These residues differ significantly from those in the equivalent locations in CYP108A1, with Val80, Thr82, Gly86, Ala90 and Leu100 in CYP108D1 replacing Ile78, Tyr80, Asn84, Met88 and Val98 in CYP108A1, resulting in a wider, more hydrophobic channel in CYP108D1 (Supplementary Table S1 and Fig. 1*e*).

At the bottom of this channel is the active site, which is defined by the residues Thr79, Val101, Ser103, Val105, Gln106, Phe190, Ile265, Ser268, Ala269, Asp272, Thr273, Val316, Phe319, Phe416 and Val417 (Figs. 2*a*, 2*b* and S5). The active sites of CYP108A1 and CYP108D1 are broadly similar (Supplementary Fig. S5 and Table S2). However, Thr79 and Val105 in CYP108D1 align with Glu77 and Thr103 in CYP108A1, resulting in a more hydrophobic active site (Figs. 2*a* and S5). Additionally, Val101, Gln106, Ile265 and Ser268 align with Ile99, Ser104, Ala263 and Thr266, and the side chains of Phe190 and Gln106 of CYP108D1 protrude further into the active-site pocket than their counterparts in CYP108A1 (Phe188 and Ser104). The α-terpineol hydroxyl

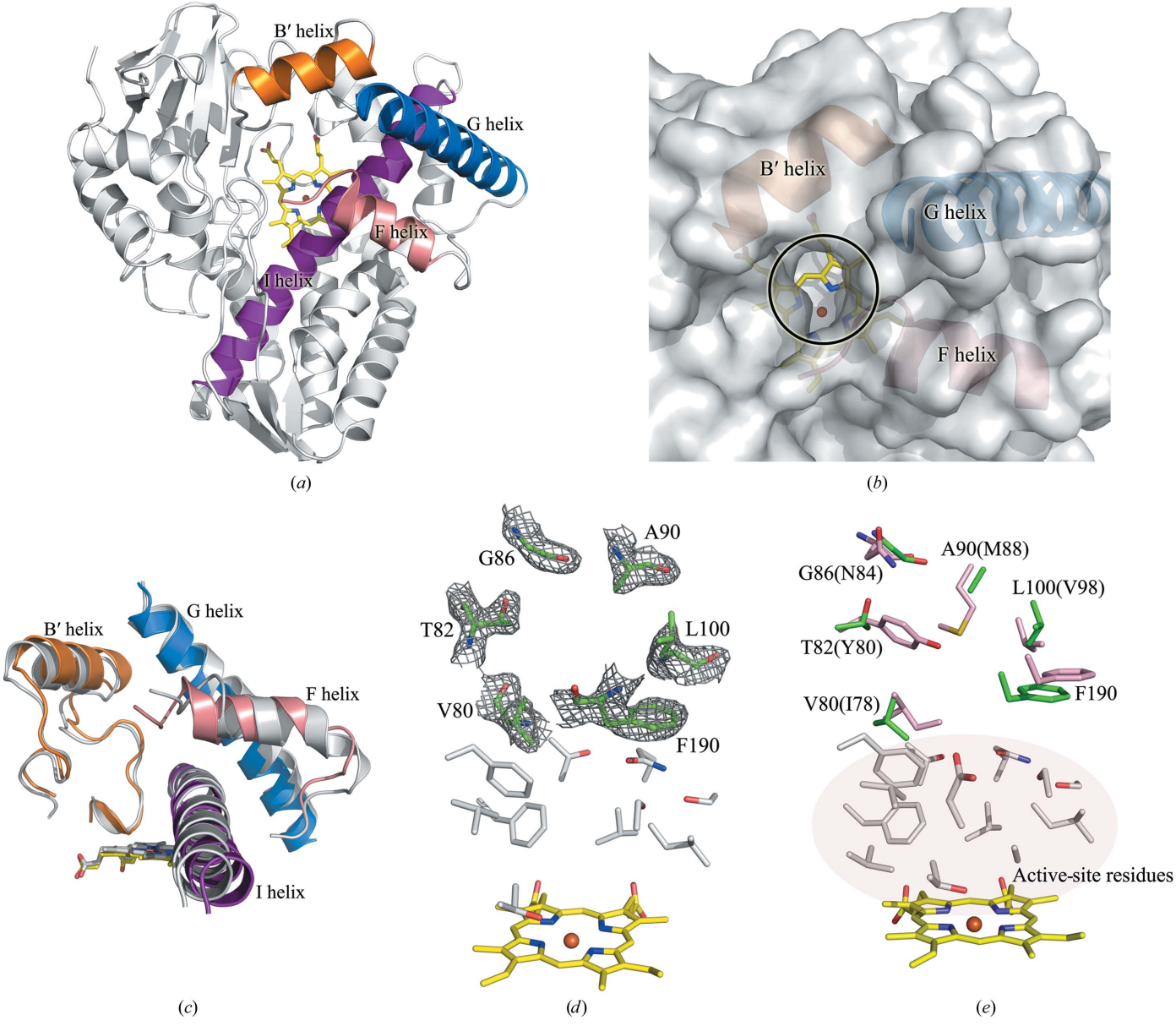

Figure 1
(*a*) The overall structure of CYP108D1. The *B*′, *F* and *G* helices are coloured orange, salmon and blue, respectively. The haem is shown in yellow and the long *I* helix (magenta) is also labelled. (*b*) The entrance to the access channel on the distal surface of CYP108D1. The *B*′, *F* and *G* helices define the entrance to the access channel, which is highlighted by the black circle. (*c*) Superposition of the *B*′, *F*, *G* and *I* helices and the haems of CYP108D1 and CYP108A1 (grey). In general, these regions overlay well, with the exception of the N-terminus of the *F* helix, which has a different orientation in CYP108D1. (*d*) The $2mF_o - DF_c$ density of the access-channel residues contoured at ∼0.35 e A^{-3}. (*e*) Comparison of the access channels of CYP108D1 (green) and CYP108A1 (pink). The haem and the active-site residues of CYP108D1 are shown in yellow and grey, respectively. The active-site residues are shown inside the oval. The access channel of CYP108D1 is lined by smaller and more hydrophobic residues. Residue differences in CYP108A1 are shown in parentheses (Supplementary Table S1).

group has been modelled as binding to Glu77 and Thr103 of CYP108A1 (Hasemann *et al.*, 1994) and the replacement of these residues by Thr79 and Val105 would contribute to the weaker binding of this substrate by CYP108D1. α-Terpineol shifts the CYP108D1 haem spin state to 40% high spin, with K_d being 156 $\pm$ 13 μM, compared with >95% shift and an association constant of 2.2×10^6 M with CYP108A1 (Peterson *et al.*, 1992). Aromatic compounds such as phenanthrene (90%), fluorene (70%), *p*-cymene (60%) and naphthalene (50%) induce larger shifts and show tighter binding with CYP108D1 than α-terpineol (Table 3; Bell & Wong, 2007). The more hydrophobic and spacious nature of the access channel and active site is consistent with the ability of CYP108D1 to bind these molecules.

The thiolato side chain of Cys379 (Fe—S = 2.3 Å) is the proximal ligand to the haem iron, which is 0.2 Å out of the porphyrin plane towards Cys379 in CYP108D1 compared with 0.05 Å in CYP108A1. The active site and access channel of the substrate-free forms of most CYP enzymes are occupied by water molecules (Poulos *et al.*, 1986; Denisov *et al.*, 2005; Pylypenko & Schlichting, 2004). Only two ordered water molecules could be modelled in the active site of CYP108D1 (Figs. 2*c* and 3*d*). Wat266 is loosely associated with the haem iron (3.3 Å) and is offset from an axial position with an S—Fe—O angle of 161° (2.1 Å and 175° in CYP108A1). The haem of substrate-free CYP108D1 appears to be fully low spin, with a Soret maximum at 419 nm (Supplementary Fig. S6). Wat266 is hydrogen bonded to Wat267 (2.4 Å) and the carbonyl of Ala269 (3.5 Å) and presumably contributes to the low-spin-state haem iron in the substrate-free form. From the crystal structure it is unclear whether there are other unresolved water molecules in the active site which could interact with Wat266. The crystal may hold CYP108D1 in an open conformation which may be differently solvated to a

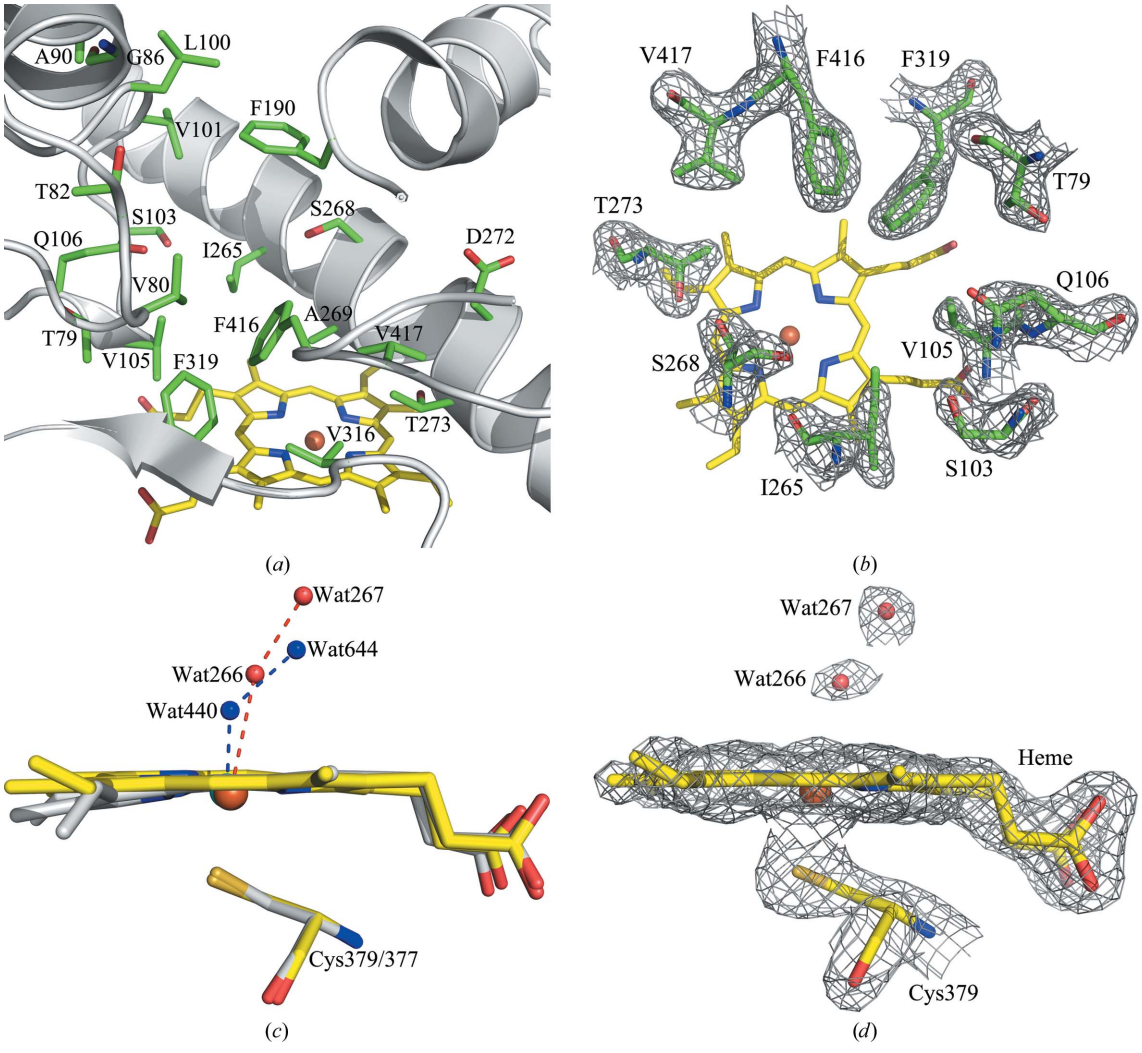

Figure 2
(*a*) The active site of CYP108D1. The residues located in the active site are shown in green. The identity and positioning of these residues are very similar to those of CYP108A1 (Supplementary Table S2 and Fig. S5). (*b*) The $2mF_o - DF_c$ density of the active-site residues contoured at ~0.35 e Å^{-3}. (*c*) Overlay of the haem and the active-site waters of CYP108D1 (yellow, with water molecules in red and the haem iron in orange) and CYP108A1 (grey, with water molecules in blue and the haem iron in cyan). Wat266 in CYP108D1 is offset from the Fe—S bond, and the Fe—O bond is longer and weaker compared with that to Wat440 in CYP108A1. (*d*) The $2mF_o - DF_c$ density of the haem, Cys379 residue and the active-site water molecules contoured at ~0.35 e Å^{-3}.

Table 3
Substrate-binding data for CYP108D1.

Substrate	High-spin haem (%)	K_d (μ*M*)
Phenylcyclohexane	95	1.01 ± 0.06
Phenanthrene	90	2.06 ± 0.10
Biphenyl	85	7.30 ± 0.21
Fluorene	70	5.85 ± 0.18
p-Cymene	60	33.8 ± 4.2
Naphthalene	50	46.9 ± 2.8
α-Terpineol	40	156 ± 13

closed conformation found in solution. Other possible explanations could be that the crystal may have trapped an unusual ferric high-spin state (in the absence of substrate) or that the haem iron may have been photoreduced to the ferrous form in the X-ray beam.

Asp272 and Thr273 are the *I*-helix acid–alcohol pair of residues which are important in oxygen activation by P450 enzymes (Denisov *et al.*, 2005; Nagano & Poulos, 2005; Vidakovic *et al.*, 1998). The backbone carbonyl of Asp272 forms a hydrogen bond to the main-chain NH of Ala276. This orientation is similar to that found in ferric substrate-free CYP108A1 (Asp270 and Ser274), CYP101D1 (Asp258 and Asn262), CYP101D2 (Asp257 and Asn261) and CYP101C1 (Asp237 and Ala241) and the ferrous-oxy form of CYP101A1 (Asp251 and Asn255) (Hasemann *et al.*, 1994; Yang *et al.*, 2010, 2011; Ma *et al.*, 2011; Schlichting *et al.*, 2000). There is a potential short path for proton delivery in CYP108D1 that leads from the *I*-helix groove to the protein surface (Zhao *et al.*, 2005). One water molecule (Wat37) is observed above the *I*-helix groove and hydrogen bonds to the carbonyl of Ser268 and the backbone N atom of Asp272. One O^{δ} atom of Asp272 is hydrogen bonded to Wat163, which is attached to a chain of water molecules that extends into the bulk solvent (Wat163–Wat206–Wat240–Wat165–Wat49–Wat17; Supplementary Fig. S7).

3.3. The substrate range of CYP108D1

A variety of hydrophobic and aromatic substrates were tested for type I spectral shifts upon binding to CYP108D1. Substrates containing up to three aromatic rings were found to bind to CYP108D1, *e.g.* phenanthrene, fluorene, biphenyl, *p*-cymene and phenylcyclohexane. Binding titrations showed that the tightest binding substrates generally induced a greater shift of the haem spin state to high spin (Table 3). For example, phenylcyclohexane binding exhibited the largest shift (95% high-spin haem) and the tightest binding (K_d = 1.01 ± 0.06 μ*M*), while biphenyl, naphthalene and α-terpineol induced smaller shifts in the haem-iron spin state and were correspondingly less tightly bound (Table 3, Figs. 3, S8 and S9). Phenanthrene showed tighter binding and induced a larger spin-state shift than fluorene and naphthalene, while other substrates such as pyrene (≤5%) and diphenylmethane (20%) induced lower spin-state shifts (Supplementary Fig. S8).

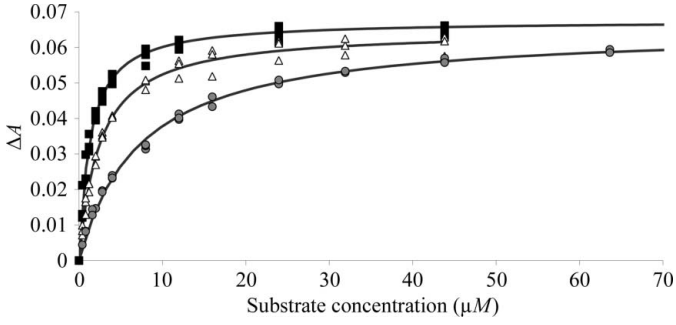

Figure 3
Substrate-binding titrations for CYP108D1 with phenanthrene (white triangles), biphenyl (grey circles) and phenylcyclohexane (black squares). Aliquots of a 1, 10 or 100 m*M* stock solution of substrate (0.5–2 μl) were added to ∼0.6 μ*M* CYP108D1 in 50 m*M* Tris pH 7.4. The tight-binding equation was used for phenylcyclohexane and phenanthrene.

The ability of CYP108D1 to bind these highly insoluble hydrophobic organic molecules would allow it to be used as an aromatic hydrocarbon monooxygenase in biocatalysis or bioremediation (Bell *et al.*, 2003, 2007; Bernhardt, 2006). Given the similar overall structure and active-site architecture of CYP108D1 and CYP108A1, the different substrate-binding profiles of the two enzymes is intriguing. The CYP108 family is abundant among bacteria, *e.g.* members can be found in *Erythrobacter*, *Sphingobium*, *Caulobacter*, *Cupriavidus*, *Burkholderia*, *Frankia* and *Mycobacterium* species (Supplementary Fig. S10). The CYP108D and CYP108A subfamilies are small compared with the CYP108B subfamily, to which the majority of the members belong (Supplementary Fig. S10; Fischer *et al.*, 2007). Further investigation will be required to ascertain the substrate-binding profiles of the other CYP108 enzymes.

The haem spin-state equilibrium in CYP108D1 was further investigated using EPR spectroscopy. Substrate-free CYP108D1 was predominantly low spin (Supplementary Fig. S11). A small contribution from a high-spin species could be observed in CYP108D1 when compared with substrate-free CYP101A1, which is fully low spin under similar conditions (Supplementary Fig. S11). The EPR spectrum of phenylcyclohexane-bound CYP108D1 indicated that there was a shift of the haem spin state from low to high spin, although a significant low-spin population was retained at 20 K despite the large spin-state shift detected by UV–Vis spectroscopy at 303 K (Supplementary Fig. S8). The CYP101A1 control sample also did not shift completely to a high-spin population on camphor binding at 20 K, which is in agreement with published data (Lipscomb, 1980).

Substrate soaking and cocrystallization experiments of CYP108D1 with identified substrates, including phenylcyclohexane, naphthalene and α-terpineol, were unsuccessful and we were unable to obtain diffracting crystals. Substrate-docking simulations were therefore performed to provide insight into potential binding orientations of phenylcyclohexane and phenanthrene. Of the calculated docking results, the lowest energy orientations were used to analyze the binding modes. Two of these were found for phenylcyclohexane (Supplementary Fig. S12*a* and Table S3) and in both modes the phenyl ring interacts with the side chains of Phe190 and Phe416. In both binding orientations the aliphatic cyclohexyl ring is nearest to the haem, with the C4 carbon

being the closest to the haem iron, which is consistent with the observed products of phenylcyclohexane oxidation by CYP108D1 (see below). Phenanthrene is modelled in the active site in a similar orientation to one of the binding modes of phenylcyclohexane, with the plane of the molecule almost perpendicular to the haem. The phenanthrene interacts with Phe190, Phe319 and Phe416 (Supplementary Fig. S12*b* and Table S4). With the caveat that significant conformational changes of CYP108D1 are likely to occur on substrate binding (Yang *et al.*, 2011; Lee *et al.*, 2010; Savino *et al.*, 2009; Wilderman *et al.*, 2010), resulting in a more closed structure and changes in the orientation of the amino-acid side chains, the aromatic residues of CYP108D1 (Phe190, Phe319 and Phe416) appear to be important in substrate binding. For both phenylcyclohexane and phenanthrene the Phe190 side chain appears to function as a cap at the top of the active site (Supplementary Fig. S12).

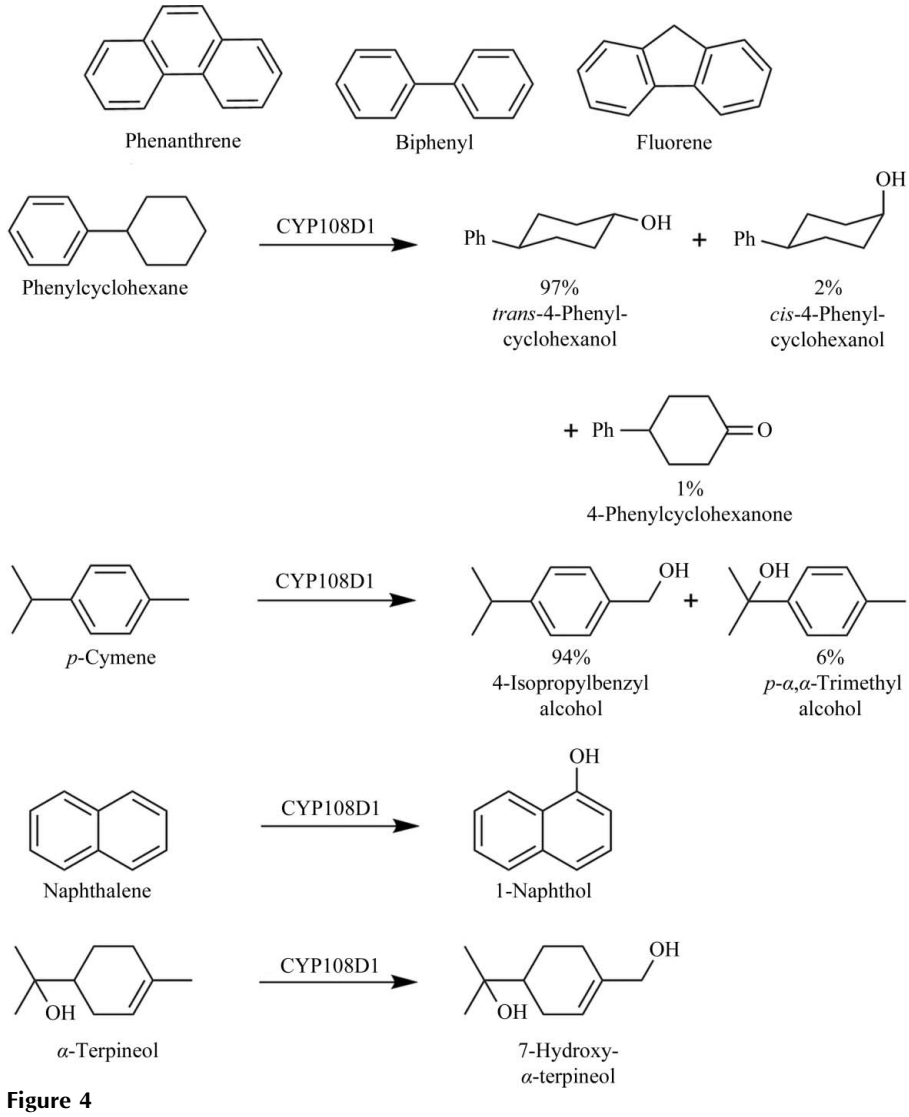

Figure 4
Substrates that bind to CYP108D1. Where identified, the oxidation products from CYP108D1 turnover are included.

3.4. The proximal face of CYP108D1 and implications for enzyme activity

The binding site for the electron-transfer partner is located on the proximal surface of P450 enzymes and a model of the CYP101A1–Pdx complex has been reported (Pochapsky *et al.*, 1996; Kuznetsov *et al.*, 2006). In *N. aromaticivorans* an ArR–Arx class I electron-transfer system supports high monooxygenase activity (k_{cat} of up to 91 s^{-1}) of CYP101B1, CYP101C1, CYP101D1, CYP101D2 and CYP111A2, but its activity with CYP108D1 was lower by three orders of magnitude (Bell, Dale *et al.*, 2010; Bell & Wong, 2007; Yang *et al.*, 2010). NADH consumption rates with substrates such as phenylcyclohexane and phenanthrene, which induce >90% high-spin haem content, were indistinguishable from the background rate in the absence of substrate [15–20 nmol min^{-1} (nmol P450)$^{-1}$]. The amount of product detected by gas chromatography (GC) from these assays was also very low. It seems unlikely that Arx is the physiological redox partner of CYP108D1. Other electron-transfer systems, including putidaredoxin reductase (PdR) and putidaredoxin (Pdx) from *P. putida* and palustrisredoxin reductases (PuR and HaPuR) and palustrisredoxins (Pux, PuxB and HaPux) from *R. palustris* CGA009 and HaA2, also gave low activities (Bell, Xu *et al.*, 2010; Bell, Tan *et al.*, 2010; Peterson *et al.*, 1990). Terpredoxin (Tdx), the physiological electron-transfer partner of CYP108A1, was tested using ArR as the ferredoxin reductase, but the activities were also nugatory. Electron transfer from ArR to Tdx was confirmed to be efficient by a cytochrome *c* reduction assay (Aoki *et al.*, 1998; Lambeth *et al.*, 1979; Bell, Xu *et al.*, 2010). The reduction of Tdx by ArR was found to have a k_{cat} of 300 $\pm$ 17 s^{-1} and K_M of 5.9 $\pm$ 1.2 μM, compared with 280 $\pm$ 12 s^{-1} and 2.9 $\pm$ 0.4 μM for Arx reduction by ArR (Yang *et al.*, 2010), clearly establishing that Tdx is unable to transfer electrons efficiently to CYP108D1.

Despite the low activities, it was possible to generate sufficient product for detection *via* gas chromatography (GC) using an *in vitro* cofactor-regeneration system (Fig. 4). Unfortunately, the amount of material was not sufficient for detailed chemical characterization, but the products could be identified *via* GC co-elution experiments using authentic standards. Phenylcyclohexane was oxidized to *trans*-4-phenylcyclohexanol (97%), with *cis*-4-phenylcyclohexanol (2%) and 4-phenylcyclohexanone (1%) being formed as minor products (Supplementary Fig. S13). The selectivity of

phenylcyclohexane oxidation is in agreement with the orientation predicted from computer-modelling calculations (Supplementary Fig. S12*a*). *p*-Cymene was predominantly oxidized to 4-isopropylbenzyl alcohol (94%), with *p*-α,α-trimethylbenzylalcohol making up the remainder. Naphthalene oxidation resulted in very low levels of 1-naphthol formation (data not shown) and several other unidentified products, while α-terpineol yielded 7-hydroxyterpineol (the same product as obtained with CYP108A1; Supplementary Fig. S13). The remaining substrates, biphenyl, fluorene and phenanthrene, all produced very low levels of products which could not be identified from the standards available (2-phenanthrol, 9-phenanthrol, 9,10-phenanthenequinone, 9-hydroxyfluorene, 9-fluorenone, 2-hydroxybiphenyl, 3-hydroxybiphenyl and 4-hydroxybiphenyl; data not shown).

Given the low activities observed with all of the [2Fe–2S] electron-transfer ferredoxins tested, we compared the proximal faces of the CYP108 and CYP101 families of enzymes (Figs. 5*a* and S14*a*). Directly beneath the haem, the electrostatic potential of the proximal face of CYP108D1 is less positively charged than those of CYP101C1, CYP101D1 and CYP101D2. However, it is more positively charged than these enzymes (and CYP101A1) around the periphery. Electrostatic interactions have been proposed to play an important role in binding between Arx and CYP101C1, CYP101D1 and CYP101D2, with the positively charged proximal faces of the CYP enzymes interacting with negatively charged residues on Arx (Yang *et al.*, 2010; Ma *et al.*, 2011; Yang *et al.*, 2011). Gln378 of CYP108D1, which is the residue preceding the haem-iron-bound Cys379, replaces arginine residues in CYP101C1, CYP101D1 and CYP101D2 but aligns with Leu356 in CYP101A1 and Met376 in CYP108A1 (Supplementary Table S5). Asp121 of CYP108D1 creates a negatively charged region on the haem-proximal face and aligns with positively charged Lys residues in the *N. aromaticivorans* CYP101 enzymes (Gln117 in CYP101A1 and Asn119 in CYP108A1; Supplementary Table S5). These residue differences may have an impact on Arx–CYP108D1 binding and electron transfer.

The region before the proximal loop, Pro365–Arg368 in CYP108D1, protrudes from the proximal surface, with the largest deviation at Ala366 and Gln367 such that Gln367 is located over the haem, unlike in CYP108A1 (Figs. 5*b*–*e* and S14*b*). Pro362 in CYP108A1 aligns with Pro365 in CYP108D1, but the sequences either side of these prolines are different: Pro365 follows directly from Arg364 in CYP108D1 with the sequence Arg364-Pro365-Ala366-Asn367, while in CYP108A1 it is Arg362-Phe363-Pro364-Asn365 (Supplementary Fig. S3). The structural distortion, which is not a consequence of crystal-packing interactions, may be a result of the different orientation of Pro365 and in particular the interactions of the subsequent residues with those of the *K* and *L* helices. The main-chain N atom and side-chain O atom of Asn367 form hydrogen bonds to the side chains of Glu307 and Arg386 (Fig. 5*e*). In contrast, the side chain NH_2 of Asn365 in CYP108A1 forms a hydrogen bond to the Glu308 side chain (in the *K* helix), even though Arg386 in CYP108D1 aligns with Lys384 in CYP108A1. There are also hydrogen bonds within the loop, such as those between the side chain of Arg368 and the carbonyl O atoms of Ala366 and Asn367, and water-bridged hydrogen bonds between the carbonyl O atom of Pro365 and the main-chain N atom of Arg368 and His369 may also help stabilize the unusual orientation of the loop which could hinder [2Fe–2S] ferredoxin binding (Figs. 5*b*–5*e*). When compared with CYP108A1, there are other significant differences close to this region. For example, an alanine residue (Ala374) replaces Trp372 in CYP108A1 and there are several proline residues in the vicinity of this loop in CYP108D1 which may have an effect on the secondary structure (Supplementary Fig. S3).

These differences in the topology and electrostatic potential of the CYP108D1 proximal face *versus* those of the CYP101 and CYP108A1 enzymes may result in weak interactions and therefore the low activities observed with the [2Fe–2S] ferredoxins. There is also a short protruding helix before the haem-binding proximal loop (Met338–Cys345) in CYP101C1 from the same bacterium, which results in a different surface topology compared with those of CYP101D1 and CYP101D2, which are similar to CYP108A1 and CYP101A1 (Supplementary Fig. S14*b*). A comparison of the CYP101C1 sequence with those of other CYP101-family members and CYP108A1 and CYP108D1 in this region reveals that a unique two-amino-acid insertion (Gly329-Leu330) is located before this short helix (Ma *et al.*, 2011). Additionally, a proline residue (Pro332) resides within it in a similar location to Pro365 of CYP108D1.

In order to explore whether the protruding loop is responsible for the slow electron transfer, Pro365 of CYP108D1 was replaced by valine. This would remove the rigid proline residue and potentially realign the loop, or at least make it less rigid. It was hoped that such a change would enable a rearrangement of this loop in CYP108D1 to facilitate ferredoxin binding. However, the activity of the Pro365Val mutant was not enhanced with any of the ferredoxins tested (data not shown). It is possible that the loop may not have realigned in the mutant owing to the extensive hydrogen-bonding network, which is absent for the short helix in CYP101C1, or the different location of the prolines. These differences may make the short helix in CYP101C1 more flexible than the loop in CYP108D1 and allow fast electron transfer from Arx. Alternatively, the protrusion may not be the sole or the dominant cause of the low activity.

3.5. The thermodynamics and kinetics of the first electron transfer

Ferredoxin recognition and binding determines the formation constant of the ferredoxin–CYP complex, the redox-centre separation and the reorganization energy for intra-complex electron transfer. Non-optimal binding orientations of a nonphysiological ferredoxin might require conformation changes in the activation step which will increase the activation energy of electron transfer. The electron-transfer rate constant is also affected by the ther-

modynamic driving force for the reaction (Sligar & Gunsalus, 1976).

The reduction potentials of substrate-free CYP108D1 and the phenylcyclohexane complex were determined by spectroelectrochemical titrations. The low-spin substrate-free form showed a reduction potential of -432 ± 8 mV (Fig. 6*a*), which is within the range commonly observed for P450 enzymes (Whitehouse *et al.*, 2011; McLean *et al.*, 2006). The potential

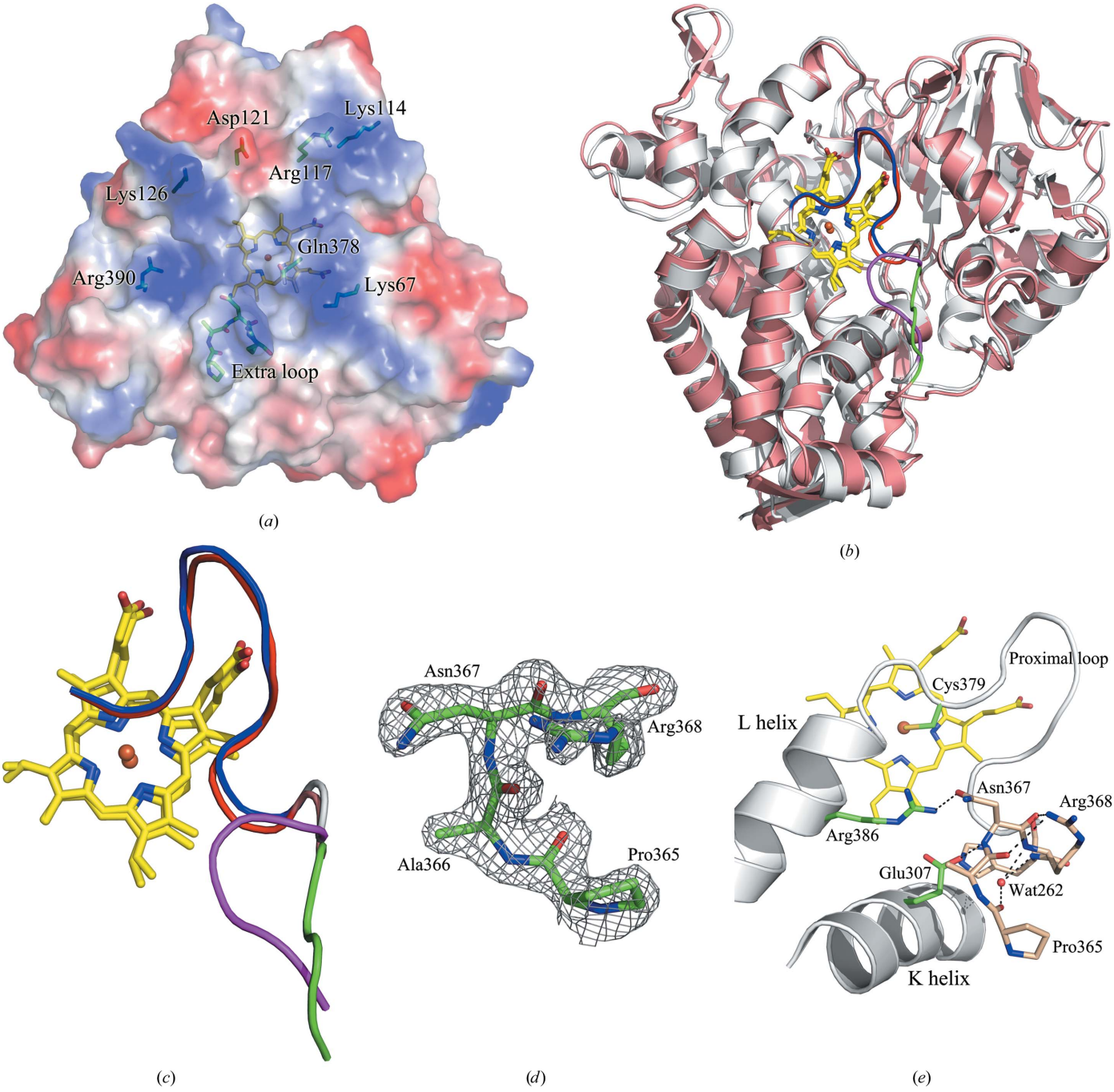

Figure 5
(*a*) The electrostatic potential of the proximal face of CYP108D1. Positively and negatively charged regions are shown in blue and red, respectively. Positively charged residues and those which align with positively charged residues in CYP101C1, CYP101D1 and CYP101D2 are labelled (Supplementary Fig. S14*a*). (*b*) A proximal-face comparison of CYP108D1 (grey) and CYP108A1 (salmon), highlighting the similar positioning of the proximal loop (shown in blue in CYP108D1 and red in CYP108A1) and the different orientation of the loop region from residues Pro365 to Arg368 of CYP108D1 (shown in magenta in CYP108D1 and green in CYP108A1). (*c*) A close-up view of the orientation of the loop region from residues Pro365 to Arg368, the proximal loop and the haem of CYP108D1 compared with CYP108A1 (coloured as in *b*). (*d*) The $2mF_o - DF_c$ density of the loop region from residues Pro365 to Arg368 contoured at -0.35 e Å^{-3}. (*e*) The orientation of the loop region from residues Pro365 to Arg368 in CYP108D1 (wheat) differs significantly from that in other CYP enzymes and leads to a different topology of the proximal face. Pro365 forces the loop to protrude out from the proximal face where it interacts with the *K* and *L* helices. The hydrogen bonds between these regions and within the loop are shown as dashed lines, with the bridging water molecules highlighted in red.

for the phenylcyclohexane complex (95% high-spin haem) was found to be −401 ± 4 mV (Fig. 6*b*). This highly reducing potential is unusual since a shift of the P450 haem spin state to high spin is commonly associated with changes in haem ligation and as a consequence the reduction potential shifts to more oxidizing values, *e.g.* the potential of CYP101A1 shifts from −300 to −170 mV on camphor binding and that of $P450_{BM3}$ shifts from −449 to −317 mV on palmitate binding (Gunsalus *et al.*, 1973; Whitehouse *et al.*, 2010).

The redox potential of Arx was determined to be −248 ± 14 mV (Fig. 6*c*) and therefore the reduction of phenylcyclohexane-bound CYP108D1 is endoergic by ∼170 meV. Even with oxygen binding to the ferrous deoxy species, the overall equilibrium constant for the formation of the ferrous-oxy intermediate from the ferric haem–substrate complex will be small, since the binding constant for oxygen is typically 10^3–10^4 M^{-1} and hence the macroscopic observed turnover rate will be lower (Honeychurch *et al.*, 1999). For comparison, the reduction potential of Pdx is −240 mV, increasing to −190 mV in the Pdx–CYP101A1 complex (Martinis *et al.*, 1996; Sligar & Gunsalus, 1976). The redox potentials of substrate-free and camphor-bound CYP101D1, which has a high activity with the ArR–Arx electron-transfer system, were found to be −419 ± 15 and −205 ± 10 mV, respectively (Fig. 6*d*), suggesting that a similar substrate-gating mechanism for the first electron-transfer step to that observed with CYP101A1 is in operation (Sligar & Gunsalus, 1976).

The reasons behind the small shift in the redox potential of CYP108D1 on substrate binding are unclear. The crystal structure shows only two ordered water molecules in the active site, with Wat266 being offset from the haem iron, although other disordered water molecules may be present. The electronic spectra and redox potential at ambient temperature show that the haem in the substrate-free form is almost entirely low spin (Figs. 6 and S6) and the low-temperature EPR spectra show only a minor contribution from a high-spin haem (Supplementary Fig. S11). The small change in redox potential on substrate binding despite the

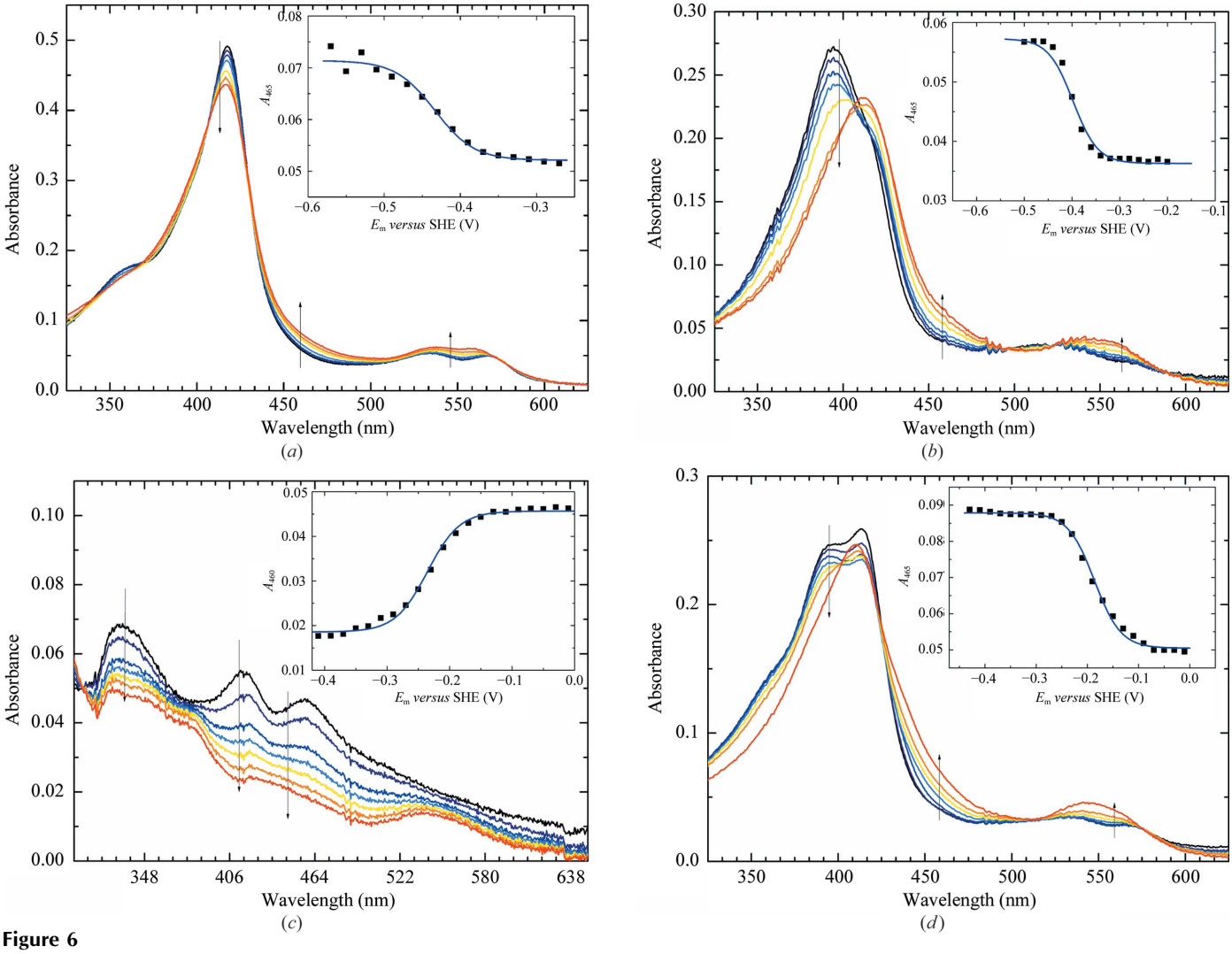

Figure 6
Mediated equilibrium spectroelectrochemical titrations of (*a*) substrate-free CYP108D1, (*b*) phenylcyclohexane-bound CYP108D1, (*c*) Arx and (*d*) camphor-bound CYP101D1. In each case, the black line is the fully oxidized form of the enzyme and the red line is the fully reduced form, with interim titrations being shown in other colours and the arrows indicating the sense in which the spectral features change as the haem iron is reduced. The insets show nonlinear least-squares fits of absorbance at 465 nm to a sigmoidal form of the Nernst equation with the number of electrons fixed at one.

change in the haem spin state from low to high spin may be linked to the low number of water molecules in the active site and the offset nature of the Fe^{II}-bound water or the out-of-plane haem iron. It has been postulated that an offset distal water may lead to a lower reorganization energy, which should assist in substrate binding (Honeychurch *et al.*, 1999; Whitehouse *et al.*, 2009). Such an offset water molecule coupled to an out-of-plane haem iron has been observed in structures of the substrate-bound form of the wild type and the I401P mutant of the CYP102A1 enzyme. However, in both of these forms of CYP102A1 the spin-state equilibrium is shifted significantly towards high spin and the reduction potential is more oxidizing (*e.g.* –302 mV for I401P; Haines *et al.*, 2001; Whitehouse *et al.*, 2009). If the number of water molecules in the active site of CYP108D1 is low, substrate binding and dehydration would induce less of a change in the polarity, which could lead to a smaller increase in the redox potential.

The volume of the active site was calculated to be 190 $Å^3$ (using *VOIDOO*) and excess disordered water in the absence or the presence of substrate (phenylcyclohexane, 174 $Å^3$; phenanthrene, 172 $Å^3$) may be freer to interact with the polar haem surface and stabilize the ferric state (Supplementary Fig. S15; Kleywegt & Jones, 1994). However, this volume may be reduced if the enzyme has a more closed conformation in the presence of substrate in solution. Using *VOIDOO*, the volume of the active site of CYP108A1 was calculated to be 225 $Å^3$, which is slightly larger than that for CYP108D1. For comparison, the active-site volumes of other CYP enzymes are CYP101A1 (P450cam; PDB entry 1phc; Poulos *et al.*, 1986), 79 $Å^3$; CYP2E1 (PDB entry 3e6i; Porubsky *et al.*, 2008), 190 $Å^3$; CYP2A6 (PDB entry 1z10; Yano *et al.*, 2005), 230 $Å^3$; CYP1A2 (PDB entry 2hi4; Sansen *et al.*, 2007), 406 $Å^3$; CYP3A4 (PDB entry 1tqn; Yano *et al.*, 2004), 1508 $Å^3$ (McLean *et al.*, 1998, Porubsky *et al.*, 2008). The lower reduction potential of substrate-free CYP108D1 may also result from differences in the active-site and haem-ligation environment, which have been proposed to be important in determining the spin state and therefore the redox potential of P450 enzymes (Loew & Harris, 2000). Alternatively, other substrates may be required to induce a larger shift in the redox potential and therefore promote electron transfer.

The endoergicity of the electron-transfer step also increases the activation energy, according to the Marcus equation. However, the reorganization energy (typically 1–1.5 eV) is the dominant factor and the rate of the forward electron-transfer step can be significant even for unfavourable driving forces (Honeychurch *et al.*, 1999). Therefore, the rate constant for formation of the $Fe^{II}(CO)$ complex (k_f) *via* ferredoxin-to-haem electron transfer followed by rapid trapping by CO was determined for the Arx–CYP108D1–phenylcyclohexane and Arx–CYP101D1–camphor reactions. Since CO binding is much faster than the electron-transfer step, k_f is an acceptable surrogate for k_{et}, the intra-complex electron-transfer rate constant.

Stopped-flow experiments showed that the first electron-transfer rate of Arx–CYP108D1 with phenylcyclohexane is negligible, which agrees with the slow NADH consumption (Supplementary Fig. S16). The behaviour of the Arx–CYP101D1–camphor system is more typical of a class I electron-transfer system. The data show a fast phase associated with the active camphor-bound enzyme (Supplementary Fig. S16). The k_f value for the fast phase was $22.9 \pm 0.8\ s^{-1}$ (1 μM P450, 2.5 μM Arx), compared with an NADH-consumption rate of $30.8 \pm 0.6\ s^{-1}$ (0.5 μM P450, 5 μM Arx) and a k_{cat} of $41 \pm 0.6\ s^{-1}$ (Yang *et al.*, 2010). The observed rate of the first electron-transfer step therefore reflected the NADH-consumption activities of CYP101D1 and CYP108D1 with the ArR–Arx electron-transfer system.

One possibility is that CYP108D1 utilizes a ferredoxin with a greater reducing potential. The genome sequence of *N. aromaticivorans* reveals that many other potential ferredoxin genes are present, *e.g.* 12 [2Fe–2S] and six [4Fe–4S] ferredoxins are found. While these are not associated with CYP108D1, they are possible electron-transfer partners. Alternatively, CYP108D1 may utilize a different electron-transfer system which may not contain an Fe–S ferredoxin (Hannemann *et al.*, 2007; Hawkes *et al.*, 2002).

In summary, CYP108D1 from *N. aromaticivorans* and CYP108A1 (P450terp) share a similar fold and both have an affinity for α-terpineol. However, both the access channel and the active site of CYP108D1 are more hydrophobic. Furthermore, the access channel of CYP108D1, which is important for substrate recognition and capture, is more spacious compared with that of CYP108A1. Consequently, CYP108D1 has a preference for more hydrophobic substrates, including aromatic hydrocarbons with up to three fused rings. The docking of phenylcyclohexane and phenanthrene into the active site predicts the binding mode of these aromatic compounds and for phenylcyclohexane agrees with the product profile observed. Hydrophobic interactions, including those with three Phe residues, appear to be important in the enzyme–substrate interaction. The redox potential of CYP108D1 does not shift by as much as expected when phenylcyclohexane binds, resulting in unfavourable thermodynamics with [2Fe–2S] ferredoxins for the first electron-transfer step. There are also electrostatic and topological differences on the CYP108D1 proximal face which may result in poor complementarity with the tested ferredoxins, resulting in the low activities observed. An alternative ferredoxin or a nonferredoxin electron-transfer partner is required to optimize the activity of CYP108D1. CYP108D1 has the potential to be used as an aromatic hydrocarbon monooxygenase in biocatalysis or bioremediation and may play a role in the metabolism and degradation of aromatic compounds by *N. aromaticivorans*. Efforts are continuing to further determine its substrate range and to find an efficient electron-transfer system.

We thank Professor Tom Pochapsky (Brandeis University, USA) for providing the terpredoxin clone and Demet Sirim (University of Stuttgart, Germany) for assistance in constructing the phylogenetic tree of the CYP108 family. This work was supported by grants 2007CB914301 (to WZ and

MB) and 2010CB530100 (to WZ) from the Ministry of Science and Technology of China Project 973, 31170684 (to WZ) from the Natural Science Foundation of China, and from the Natural Sciences and Engineering Research Council (NSERC, Canada) and the Rhodes Trust (both to JY).

References

Aoki, M., Ishimori, K. & Morishima, I. (1998). *Biochim. Biophys. Acta*, **1386**, 168–178.

Bell, S. G., Chen, X., Xu, F., Rao, Z. & Wong, L.-L. (2003). *Biochem. Soc. Trans.* **31**, 558–562.

Bell, S. G., Dale, A., Rees, N. H. & Wong, L.-L. (2010). *Appl. Microbiol. Biotechnol.* **86**, 163–175.

Bell, S. G., Harford-Cross, C. F. & Wong, L.-L. (2001). *Protein Eng.* **14**, 797–802.

Bell, S. G., Hoskins, N., Whitehouse, C. J. C. & Wong, L.-L. (2007). *The Ubiquitous Roles of Cytochrome P450 Proteins*, edited by A. Sigel, H. Sigel & R. K. O. Sigel, pp. 437–476. New York: Wiley.

Bell, S. G., Rouch, D. A. & Wong, L.-L. (1997). *J. Mol. Catal. B Enzym.* **3**, 293–302.

Bell, S. G., Tan, A. B., Johnson, E. O. & Wong, L.-L. (2010). *Mol. Biosyst.* **6**, 196–204.

Bell, S. G. & Wong, L.-L. (2007). *Biochem. Biophys. Res. Commun.* **360**, 666–672.

Bell, S. G., Xu, F., Forward, I., Bartlam, M., Rao, Z. & Wong, L.-L. (2008). *J. Mol. Biol.* **383**, 561–574.

Bell, S. G., Xu, F., Johnson, E. O., Forward, I. M., Bartlam, M., Rao, Z. & Wong, L.-L. (2010). *J. Biol. Inorg. Chem.* **15**, 315–328.

Berman, H. M., Westbrook, J., Feng, Z., Gilliland, G., Bhat, T. N., Weissig, H., Shindyalov, I. N. & Bourne, P. E. (2000). *Nucleic Acids Res.* **28**, 235–242.

Bernhardt, R. (2006). *J. Biotechnol.* **124**, 128–145.

Bluthe, N., Ecoto, J., Fetizon, M. & Lazare, S. (1980). *J. Chem. Soc. Perkin Trans. 1*, pp. 1747–1751.

Chen, V. B., Arendall, W. B., Headd, J. J., Keedy, D. A., Immormino, R. M., Kapral, G. J., Murray, L. W., Richardson, J. S. & Richardson, D. C. (2010). *Acta Cryst.* D**66**, 12–21.

Cojocaru, V., Winn, P. J. & Wade, R. C. (2007). *Biochim. Biophys. Acta*, **1770**, 390–401.

Cryle, M. J., Stok, J. E. & De Voss, J. J. (2003). *Aust. J. Chem.* **56**, 749–762.

Denisov, I. G., Makris, T. M., Sligar, S. G. & Schlichting, I. (2005). *Chem. Rev.* **105**, 2253–2277.

Dunn, A. R., Dmochowski, I. J., Bilwes, A. M., Gray, H. B. & Crane, B. R. (2001). *Proc. Natl Acad. Sci. USA*, **98**, 12420–12425.

Emsley, P. & Cowtan, K. (2004). *Acta Cryst.* D**60**, 2126–2132.

Engh, R. A. & Huber, R. (1991). *Acta Cryst.* A**47**, 392–400.

Fischer, M., Knoll, M., Sirim, D., Wagner, F., Funke, S. & Pleiss, J. (2007). *Bioinformatics*, **23**, 2015–2017.

Fredrickson, J. K., Brockman, F. J., Workman, D. J., Li, S. W. & Stevens, T. O. (1991). *Appl. Environ. Microbiol.* **57**, 796–803.

Fruetel, J. A., Mackman, R. L., Peterson, J. A. & Ortiz de Montellano, P. R. (1994). *J. Biol. Chem.* **269**, 28815–28821.

Guengerich, F. P. (2001). *Chem. Res. Toxicol.* **14**, 611–650.

Gunsalus, I. C., Meeks, J. R. & Lipscomb, J. D. (1973). *Ann. N. Y. Acad. Sci.* **212**, 107–121.

Haines, D. C., Tomchick, D. R., Machius, M. & Peterson, J. A. (2001). *Biochemistry*, **40**, 13456–13465.

Hannemann, F., Bichet, A., Ewen, K. M. & Bernhardt, R. (2007). *Biochim. Biophys. Acta*, **1770**, 330–344.

Hasemann, C. A., Kurumbail, R. G., Boddupalli, S. S., Peterson, J. A. & Deisenhofer, J. (1995). *Structure*, **3**, 41–62.

Hasemann, C. A., Ravichandran, K. G., Peterson, J. A. & Deisenhofer, J. (1994). *J. Mol. Biol.* **236**, 1169–1185.

Hawkes, D. B., Adams, G. W., Burlingame, A. L., Ortiz de Montellano, P. R. & De Voss, J. J. (2002). *J. Biol. Chem.* **277**, 27725–27732.

Honeychurch, M. J., Hill, H. A. O. & Wong, L.-L. (1999). *FEBS Lett.* **451**, 351–353.

Isin, E. M. & Guengerich, F. P. (2007). *Biochim. Biophys. Acta*, **1770**, 314–329.

Jones, N. E., England, P. A., Rouch, D. A. & Wong, L.-L. (1996). *Chem. Commun.*, pp. 2413–2414.

Kaplan, M. M. (2004). *Am. J. Gastroenterol.* **99**, 2147–2149.

Kleywegt, G. J. & Jones, T. A. (1994). *Acta Cryst.* D**50**, 178–185.

Kuznetsov, V. Y., Poulos, T. L. & Sevrioukova, I. F. (2006). *Biochemistry*, **45**, 11934–11944.

Lambeth, J. D., Seybert, D. W. & Kamin, H. (1979). *J. Biol. Chem.* **254**, 7255–7264.

Lee, Y.-T., Wilson, R. F., Rupniewski, I. & Goodin, D. B. (2010). *Biochemistry*, **49**, 3412–3419.

Li, H. & Poulos, T. L. (2004). *Curr. Top. Med. Chem.* **4**, 1789–1802.

Lipscomb, J. D. (1980). *Biochemistry*, **19**, 3590–3599.

Loew, G. H. & Harris, D. L. (2000). *Chem. Rev.* **100**, 407–420.

Ma, M., Bell, S. G., Yang, W., Hao, Y., Rees, N. H., Bartlam, M., Zhou, W., Wong, L.-L. & Rao, Z. (2011). *Chembiochem*, **12**, 88–99.

Martinis, S. A., Blanke, S. R., Hager, L. P., Sligar, S. G., Hoa, G. H., Rux, J. J. & Dawson, J. H. (1996). *Biochemistry*, **35**, 14530–14536.

McCoy, A. J., Grosse-Kunstleve, R. W., Adams, P. D., Winn, M. D., Storoni, L. C. & Read, R. J. (2007). *J. Appl. Cryst.* **40**, 658–674.

McLean, M. A., Maves, S. A., Weiss, K. E., Krepich, S. & Sligar, S. G. (1998). *Biochem. Biophys. Res. Commun.* **252**, 166–172.

McLean, K. J., Warman, A. J., Seward, H. E., Marshall, K. R., Girvan, H. M., Cheesman, M. R., Waterman, M. R. & Munro, A. W. (2006). *Biochemistry*, **45**, 8427–8443.

Mo, H., Pochapsky, S. S. & Pochapsky, T. C. (1999). *Biochemistry*, **38**, 5666–5675.

Morris, G. M., Goodsell, D. S., Halliday, R. S., Huey, R., Hart, W. E., Belew, R. K. & Olson, A. J. (1998). *J. Comput. Chem.* **9**, 1662–1939.

Murshudov, G. N., Skubák, P., Lebedev, A. A., Pannu, N. S., Steiner, R. A., Nicholls, R. A., Winn, M. D., Long, F. & Vagin, A. A. (2011). *Acta Cryst.* D**67**, 355–367.

Nagano, S. & Poulos, T. L. (2005). *J. Biol. Chem.* **280**, 31659–31663.

Omura, T. & Sato, R. (1964). *J. Biol. Chem.* **239**, 2370–2378.

Ortiz de Montellano, P. R. (2005). *Cytochrome P450: Structure, Mechanism and Biochemistry*, 3rd ed. New York: Kluwer Academic/Plenum Publishers.

Otwinowski, Z. & Minor, W. (1997). *Methods Enzymol.* **276**, 307–326.

Perrakis, A., Morris, R. & Lamzin, V. S. (1999). *Nature Struct. Biol.* **6**, 458–463.

Peterson, J. A., Lorence, M. C. & Amarneh, B. (1990). *J. Biol. Chem.* **265**, 6066–6073.

Peterson, J. A., Lu, J. Y., Geisselsoder, J., Graham-Lorence, S., Carmona, C., Witney, F. & Lorence, M. C. (1992). *J. Biol. Chem.* **267**, 14193–14203.

Pochapsky, T. C., Kazanis, S. & Dang, M. (2010). *Antioxid. Redox Signal.* **13**, 1273–1296.

Pochapsky, T. C., Lyons, T. A., Kazanis, S., Arakaki, T. & Ratnaswamy, G. (1996). *Biochimie*, **78**, 723–733.

Porubsky, P. R., Meneely, K. M. & Scott, E. E. (2008). *J. Biol. Chem.* **283**, 33698–33707.

Poulos, T. L., Finzel, B. C. & Howard, A. J. (1986). *Biochemistry*, **25**, 5314–5322.

Poulos, T. L., Finzel, B. C. & Howard, A. J. (1987). *J. Mol. Biol.* **195**, 687–700.

Pylypenko, O. & Schlichting, I. (2004). *Annu. Rev. Biochem.* **73**, 991–1018.

Romine, M. F., Stillwell, L. C., Wong, K.-K., Thurston, S. J., Sisk, E. C., Sensen, C., Gaasterland, T., Fredrickson, J. K. & Saffer, J. D. (1999). *J. Bacteriol.* **181**, 1585–1602.

Sambrook, J., Fritsch, E. F. & Maniatis, T. (1989). *Molecular Cloning: A Laboratory Manual*, 2nd ed. New York: Cold Spring Harbor Laboratory Press.
Sansen, S., Yano, J. K., Reynald, R. L., Schoch, G. A., Griffin, K. J., Stout, C. D. & Johnson, E. F. (2007). *J. Biol. Chem.* **282**, 14348–14355.
Savino, C., Montemiglio, L. C., Sciara, G., Miele, A. E., Kendrew, S. G., Jemth, P., Gianni, S. & Vallone, B. (2009). *J. Biol. Chem.* **284**, 29170–29179.
Schlichting, I., Berendzen, J., Chu, K., Stock, A. M., Maves, S. A., Benson, D. E., Sweet, R. M., Ringe, D., Petsko, G. A. & Sligar, S. G. (2000). *Science*, **287**, 1615–1622.
Sigel, A., Sigel, H. & Sigel, R. (2007). *The Ubiquitous Roles of Cytochrome P450 Proteins*. New York: Wiley.
Sligar, S. G. & Gunsalus, I. C. (1976). *Proc. Natl Acad. Sci. USA*, **73**, 1078–1082.
Takeuchi, M., Hamana, K. & Hiraishi, A. (2001). *Int. J. Syst. Evol. Microbiol.* **51**, 1405–1417.
Vidakovic, M., Sligar, S. G., Li, H. & Poulos, T. L. (1998). *Biochemistry*, **37**, 9211–9219.
Whitehouse, C. J., Bell, S. G., Yang, W., Yorke, J. A., Blanford, C. F., Strong, A. J., Morse, E. J., Bartlam, M., Rao, Z. & Wong, L.-L. (2009). *Chembiochem*, **10**, 1654–1656.
Whitehouse, C. J., Yang, W., Yorke, J. A., Rowlatt, B. C., Strong, A. J., Blanford, C. F., Bell, S. G., Bartlam, M., Wong, L.-L. & Rao, Z. (2010). *Chembiochem*, **11**, 2549–2556.
Whitehouse, C. J., Yang, W., Yorke, J. A., Tufton, H. G., Ogilvie, L. C., Bell, S. G., Zhou, W., Bartlam, M., Rao, Z. & Wong, L.-L. (2011). *Dalton Trans.*, pp. 10383–10396.
Wilderman, P. R., Shah, M. B., Liu, T., Li, S., Hsu, S., Roberts, A. G., Goodlett, D. R., Zhang, Q., Woods, V. L., Stout, C. D. & Halpert, J. R. (2010). *J. Biol. Chem.* **285**, 38602–38611.
Williams, J. W. & Morrison, J. F. (1979). *Methods Enzymol.* **63**, 437–467.
Winn, M. D. *et al.* (2011). *Acta Cryst.* D**67**, 235–242.
Xu, F., Bell, S. G., Peng, Y., Johnson, E. O., Bartlam, M., Rao, Z. & Wong, L.-L. (2009). *Proteins*, **77**, 867–880.
Yang, W., Bell, S. G., Wang, H., Zhou, W., Bartlam, M., Wong, L.-L. & Rao, Z. (2011). *Biochem. J.* **433**, 85–93.
Yang, W., Bell, S. G., Wang, H., Zhou, W., Hoskins, N., Dale, A., Bartlam, M., Wong, L.-L. & Rao, Z. (2010). *J. Biol. Chem.* **285**, 27372–27384.
Yano, J. K., Hsu, M.-H., Griffin, K. J., Stout, C. D. & Johnson, E. F. (2005). *Nature Struct. Mol. Biol.* **12**, 822–823.
Yano, J. K., Wester, M. R., Schoch, G. A., Griffin, K. J., Stout, C. D. & Johnson, E. F. (2004). *J. Biol. Chem.* **279**, 38091–38094.
Zhao, B., Guengerich, F. P., Voehler, M. & Waterman, M. R. (2005). *J. Biol. Chem.* **280**, 42188–42197.